Stanford Exploration Project, Report 114, October 14, 2003, pages 81–93

Wave-equation MVA: Born, Rytov and beyond

Paul Sava and Biondo Biondi[1]

ABSTRACT

The linearized wave-equation MVA operator can be used for velocity analysis using both Born and Rytov approximations. The distinction arises from the method used to compute the image perturbations. Both approximations suffer from limitations that limit their practicality: the Born approximation is usable only for small anomalies, while the Rytov approximation requires phase unwrapping. Differential image perturbations can be used for arbitrarily large slowness anomalies and do not require phase unwrapping, but their accuracy decreases with increasing deviation from the background image. For simple cases, the differential image perturbation method is equivalent with phase-unwrapped Rytov.

INTRODUCTION

Migration velocity analysis based on downward continuation methods, also known as *wave-equation migration velocity analysis* (WEMVA), is a technique designed as a companion to wave-equation migration (Biondi and Sava, 1999; Sava and Fomel, 2002). The main idea of WEMVA is to use downward continuation operators for migration velocity analysis (MVA), as well as for migration. This is in contrast with other techniques which use downward continuation for migration, but traveltime-based techniques for migration velocity updating (Clapp, 2001; Liu et al., 2001; Mosher et al., 2001).

WEMVA is an optimization problem where the objective function is defined in the image space. As for other MVA methods, it tries to maximize the quality of the migrated image instead of trying to match the recorded data (Sava and Symes, 2002). In this respect, our method is related to Differential Semblance Optimization (Symes and Carazzone, 1991) and Multiple Migration Fitting (Chavent and Jacewitz, 1995). However, with respect to these two methods, our method has the advantage of exploiting the power of residual prestack migration to speed up the convergence, and it also gives us the ability to guide the inversion by geologic interpretation.

WEMVA benefits from the same advantages over traveltime estimation methods as wave-equation migration benefits over Kirchhoff migration. The most important among them are the accurate handling of complex wavefields which are characterized by multipathing, and the band-limited nature of the imaging process, which can handle sharp velocity variations much better than traveltime-based methods. Complex geology, therefore, is where WEMVA

[1]**email:** paul@sep.stanford.edu, biondo@sep.stanford.edu

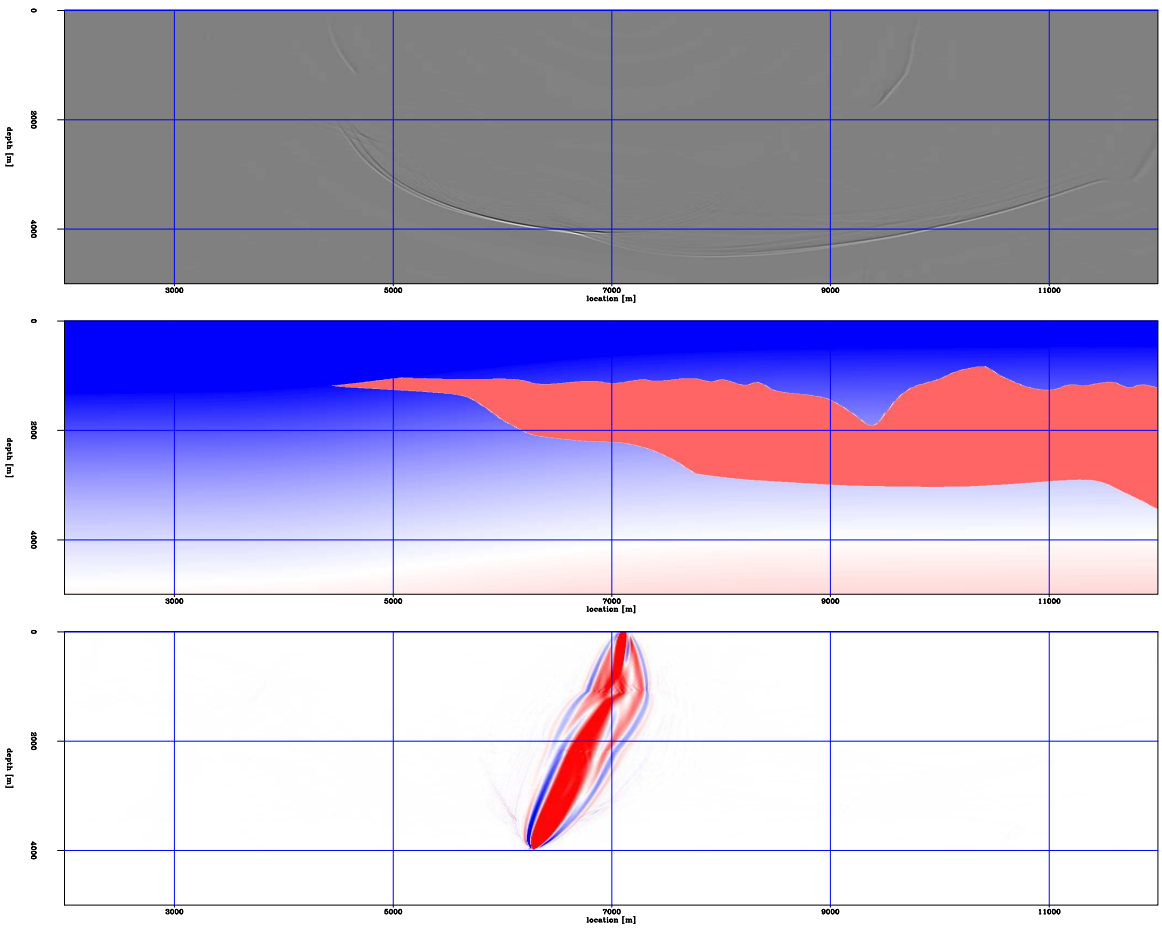

Figure 1: Fat rays in a salt velocity model. From top to bottom, the wavefield from a point source on the surface, the velocity model, and a fat ray from a point in the subsurface to the source. paul1-FRzig.sds [CR,M]

is expected to provide the largest benefits.

Figures 1 and 2 illustrate the complications encountered under salt. From top to bottom, we show the wavefield corresponding to a point-source at the surface, the background slowness model, and a "fat ray" (Woodward, 1992) from the source to a point in the subsurfaces. Both examples show multipathing between source and receiver which is naturally taken into account by WEMVA, but which cannot be handled by simple traveltime tomography. Also, the slowness model is not smooth as required by methods using ray tracing.

WEMVA is based on a linearization of the downward-continuation operator using the Born approximation. This approximation leads to severe limitations on the magnitude and size of the anomalies that can be handled. Therefore, it cannot operate successfully in the regions of highest complexity. Other methods of linearization are possible (Sava and Fomel, 2002), but none allow for arbitrarily large anomalies.

In our early tests (Biondi and Sava, 1999), we construct the image perturbation using

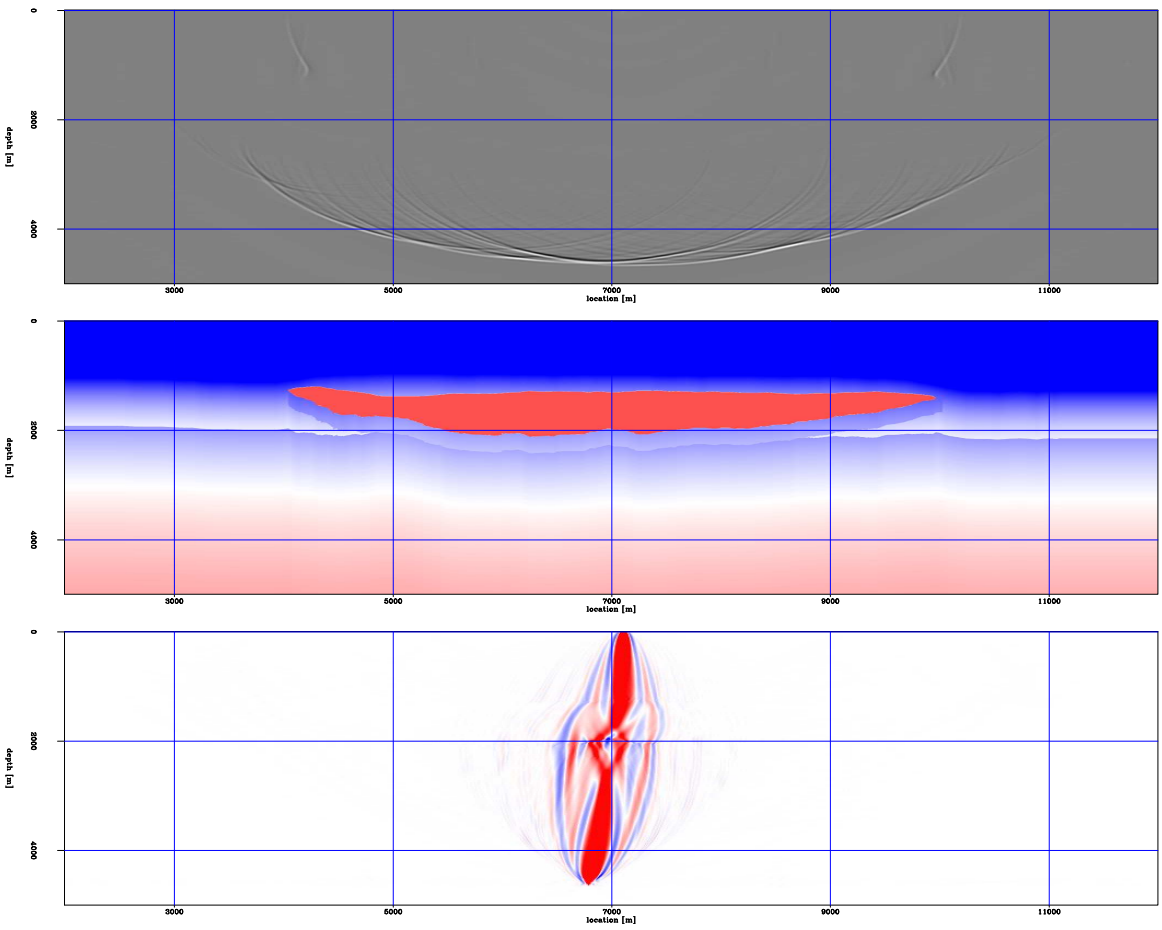

Figure 2: Fat rays in a salt velocity model. From top to bottom, the wavefield from a point source on the surface, the velocity model, and a fat ray from a point in the subsurface to the source. paul1-FRgom.sds [CR,M]

Prestack Stolt Residual Migration (PSRM) (Sava, 2003). In summary, this residual migration method provides updated images for new velocity maps that correspond to a fixed ratio (ρ) of the new velocity with respect to the original velocity map. Residual migration is run for various ratio parameters, and finally we pick the best image by selecting the flattest gathers at every point.

The main disadvantage of building the image perturbation using PSRM is that, for large velocity ratio parameters (ρ), the background and improved images can get more than $\pi/4$ out of phase. Therefore, the image perturbation computed by the Born forward operator and the one computed by residual migration are fundamentally different, and can have contradictory behaviors when using the linearized WEMVA operator for inversion.

Alternative methods can be used to create image perturbations for WEMVA, directly in compliance with the Born approximation (Sava and Biondi, 2003). Those methods are not limited by the same restrictions as the Born methods, although their accuracy decreases with increasing deviation from the reference images. We refer to image perturbations created with

this method as differential image perturbations.

In this paper we investigate various methods that can be used to compute image perturbations. Our goal is two fold: firstly, we show that we can do Rytov WEMVA basically using the same backprojection operator as the one involved in the Born approximation, but with a different definition of the image perturbation; secondly, we further investigate the differential approach to computing image perturbations and show that this method is similar to a phase-unwrapped Rytov, although it does not require any explicit phase unwrapping. Thus, the differential method is more practical and robust than a Rytov method, although it is less accurate and may require more non-linear iterations for convergence.

We begin with a review of wave-equation MVA with emphasis on the methods used to compute image perturbations. We then describe the Rytov approach to WEMVA and explore the relationship between the three different methodologies. Finally, we present a couple of synthetic examples for each of the image perturbation methods mentioned earlier and discuss the relationships between them.

WEMVA THEORY

The wavefield constructed by downward continuation from the surface to depth z, $\mathcal{U}(\omega)$ is

$$\mathcal{U} = \mathcal{D} e^{i \sum_z \Phi_z} , \tag{1}$$

where $\mathcal{D}$ is the data at the surface and Φ_z is the complex phase shift at one depth level. We can write the phase Φ_z at every depth level as a Taylor expansion around a reference medium of slowness s_o

$$\begin{aligned} \Phi_z &= \Phi_{z_o} + \left. \frac{d\Phi_z}{ds} \right|_{s=s_o} \Delta s & (2) \\ &= \Phi_{z_o} + \Delta\Phi_z \, . & (3) \end{aligned}$$

If we plug equation (2) in equation (1) we can write the following expression for the wavefield $\mathcal{U}$:

$$\mathcal{U} = \mathcal{U}_o e^{i \sum_z \Delta\Phi_z} , \tag{4}$$

where $\mathcal{U}_o$ corresponds to the background slowness s_o, and $\mathcal{U}$ corresponds to an arbitrary spatially varying slowness $s = s_o + \Delta s$.

We can define a wavefield perturbation at depth z by the expression

$$\begin{aligned} \Delta\mathcal{U} &= \mathcal{U} - \mathcal{U}_o & (5) \\ &= \mathcal{U}_o \left[e^{i \sum_z \Delta\Phi_z} - 1 \right] & (6) \end{aligned}$$

or, if we use the notation $\Delta\Phi = \sum_z \Delta\Phi_z$

$$\Delta\mathcal{U} = \mathcal{U}_o \left[e^{i\Delta\Phi} - 1 \right] . \tag{7}$$

In general, we can compute a wavefield perturbation $\Delta\mathcal{U}(\omega,z)$ by applying a non-linear operator $\mathbf{L}$ which depends on the background wavefield $\mathcal{U}_o(\omega,z)$ to a slowness perturbation $\Delta s(z)$, according to equation (7):

$$\Delta\mathcal{U} = \mathbf{L}(\mathcal{U}_o)[\Delta s] \ . \tag{8}$$

Linearization

The simplest linearization of equation (7) is done by the Born approximation, which involves an approximation of the exponential function by a linear function $e^{i\phi} = 1 + i\phi$. With this approximation, we obtain

$$\Delta\mathcal{U} \approx \mathcal{U}_o \, i\,\Delta\Phi \ . \tag{9}$$

We can, therefore, compute a linear wavefield perturbation $\Delta\mathcal{U}(\omega,z)$ using a Born WEMVA operator:

$$\Delta\mathcal{U} = \mathbf{B}(\mathcal{U}_o)[\Delta s] \ , \tag{10}$$

from which we can compute an image perturbation by summation over frequency:

$$\Delta\mathcal{R} = \sum_{\omega} \Delta\mathcal{U} \ . \tag{11}$$

For wave-equation MVA, we are interested in applying an inverse WEMVA operator to a given image perturbation. Therefore, the main challenge of the linearized WEMVA is to estimate correctly $\Delta\mathcal{R}$, i.e. an image perturbation corresponding to the accumulated phase differences given by all slowness anomalies above each image point.

Given an image perturbation $\Delta\mathcal{R}$, we can compute a wavefield perturbation $\Delta\mathcal{U}$ by the adjoint of the imaging operator, from which we can compute a slowness perturbation based on the background wavefield $\mathcal{U}_o$:

$$\Delta s = \mathbf{B}^*(\mathcal{U}_o)[\Delta\mathcal{U}] \ . \tag{12}$$

Born image perturbation

The simplest way of computing image/wavefield perturbations is by simple subtraction of the wavefields for the background image $\mathcal{U}_o$ from the wavefield of a better image $\mathcal{U}$:

$$\Delta\mathcal{U}_b = \mathcal{U} - \mathcal{U}_o \ . \tag{13}$$

Equation (13) is only valid for small perturbations of the wavefields ($\Delta\mathcal{U}_b << 1$). In practice, this requirement means that the cumulative phase difference between the two different wavefields is small at all frequencies.

If this condition is satisfied, we can compute a slowness perturbation which corresponds to the Born approximation:

$$\Delta s_b = \mathbf{B}^*(\mathcal{U}_o)[\Delta\mathcal{U}_b] \ . \tag{14}$$

In practice, the small perturbation requirement is hard to meet, since small slowness differences ammount to large cumulative phase differences. Thus, with the wavefield perturbation definition in equation (13), we can only handle small slowness perturbations.

Rytov image perturbation

An alternative to the wavefield perturbation definition in equation (13) is given by the Rytov approximation. If we can estimate the accumulated phase differences between the two wavefields at every depth level

$$\Delta\Phi_r = \Phi - \Phi_o \ , \tag{15}$$

we can compute another wavefield perturbation using the relation:

$$\Delta\mathcal{U}_r = \mathcal{U}_o \, i\Delta\Phi_r \tag{16}$$

which is directly derived from equation (9). With this definition of the wavefield perturbation, we can compute another slowness perturbation which corresponds to the Rytov approximation

$$\Delta s_r = \mathbf{B}^*(\mathcal{U}_o)[\Delta\mathcal{U}_r] \tag{17}$$

using the same backprojection operator.

Differential image perturbation

Various methods can be used to improve images created with inaccurate, reference velocity models. Residual migration (Stolt, 1996; Al-Yahya, 1989; Etgen, 1990) is one such option, although we could use other methods like residual moveout or image continuation.

If image enhancement is done with a Stolt-type residual migration operator $\mathbf{S}$ (Stolt, 1996; Sava, 2000, 2003), we can write a relation for an improved image $\mathcal{R}$ derived from a reference image $\mathcal{R}_o$

$$\mathcal{R} = \mathbf{S}(\rho)[\mathcal{R}_o] \ , \tag{18}$$

where ρ is a spatially varying scalar parameter indicating the magnitude of residual migration at every image point. We can compute a linearized image perturbation by a simple first-order expansion relative to the parameter ρ

$$\Delta\mathcal{R}_a = \left.\frac{d\mathbf{S}}{d\rho}\right|_{\rho=\rho_o} [\mathcal{R}_o] \ \Delta\rho \ , \tag{19}$$

from which we can compute a wavefield perturbation $\Delta\mathcal{U}_a$ using the adjoint of the imaging operator.

The operator $\left.\frac{d\mathbf{S}}{d\rho}\right|_{\rho=\rho_o}$ can be computed analytically, since it only depends on the background image, while $\Delta\rho$ can be picked at every location from a suite of images computed using different values of ρ (Sava and Biondi, 2003). Similar formulations are possible for

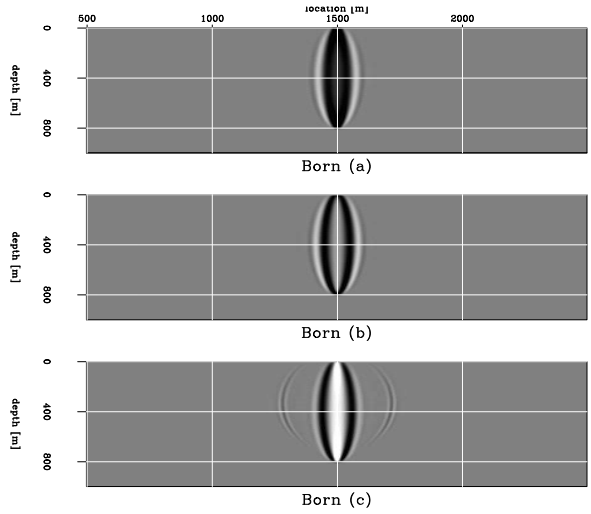

Figure 3: Fat rays for an image perturbation defined using the Born equation (21). The slowness anomaly is gradually increasing from (a) to (c). Only the smallest anomaly is correctly handled by the Born image perturbation. paul1-RYTOV3b.xbsbor [CR]

other kinds of operators (e.g., normal residual moveout), and are not restricted to residual migration, in general, or to Stolt residual migration, in particular.

With this definition of the wavefield perturbation, we can compute another slowness perturbation:

$$\Delta s_a = \mathbf{B}^*(\mathcal{U}_o)[\Delta \mathcal{U}_a] \ . \tag{20}$$

DISCUSSION

We have shown in the preceding section several methods that can be used to create image perturbations to be inverted for slowness perturbations:

$$\Delta \mathcal{R}_b = \sum_\omega (\mathcal{U} - \mathcal{U}_o) \tag{21}$$

$$\Delta \mathcal{R}_r = i \sum_\omega (\mathcal{U}_o (\Phi - \Phi_o)) \tag{22}$$

$$\Delta \mathcal{R}_a = \left. \frac{d\mathbf{S}}{d\rho} \right|_{\rho=\rho_o} [\mathcal{R}_o] \ \Delta\rho \ . \tag{23}$$

Figure 3 shows the slowness backprojection for image perturbations computed using the definition in equation (21). From top to bottom, the panels correspond to increasing magnitudes of the slowness anomalies. In panel (a), the accumulated differences between the background and correct images is small, such that the Born approximation holds and the backprojection creates simple "fat rays" (Woodward, 1992). However, as the slowness anomaly increases, the fat rays are distorted by sign changes (b), and/or by the characteristic ellipsoidal side-lobes (c).

Figure 4 shows the slowness backprojection for image perturbations computed using the definition in equation (22). From top to bottom, the panels correspond to increasing magnitudes of the slowness anomalies. In panels (a) and (b), the accumulated phase differences

between the background and correct images are small and do not wrap. Backprojection by WEMVA also creates simple undistorted fat rays. At large magnitudes, however, the phases become large enough to wrap, and backprojection from image perturbations defined by equation (22) fails (c).

Both equation (21) and equation (22) employ the same operator for backprojection. The difference is in the method we use to define the wavefield perturbation. For equation (21) we use the difference between the complete wavefields, with the constraint of small total wavefield difference. For equation (22) we use the difference between the cumulative phases, which does not impose a constraint on the actual size of the wavefields. Thus, using equation (22), we could in principle handle arbitrarily large slowness perturbations.

However, the phases in equation (22) need to be unwrapped to obtain a meaningful wavefield differences. In complex environments, wavefields are can be quite complicated, and it is not at all trivial to estimate and unwrap their phases. Therefore, even if we could in theory use equation (22) for arbitrarily large perturbations, in practice we are constrained by our ability to unwrap the phases of complicated wavefields. Figure 5 shows the fat rays corresponding to the different magnitudes of slowness anomalies when the phases have been unwrapped.

The more practical alternative we can use to create image perturbations using equation (23) is illustrated in Figure 6. In this case, the fat rays are not distorted at any magnitude of slowness anomaly, behavior which is similar to that of the unwrapped Rytov.

The explanation for this behavior lies in the definition in equation (23). The image perturbation is created by estimating the gradient of the residual migration change on the background image, followed by scaling with the appropriate $\Delta\rho$ picked from a suite of images obtained with different values of the parameter ρ.

In essence, we are using the information provided by the background image to infer the direction and magnitude of the image change. There is no limitation to how far we can go from the background image similar to the limitations of the Born and Rytov definitions. However, since we are employing a first order linearization, the accuracy of the differential image

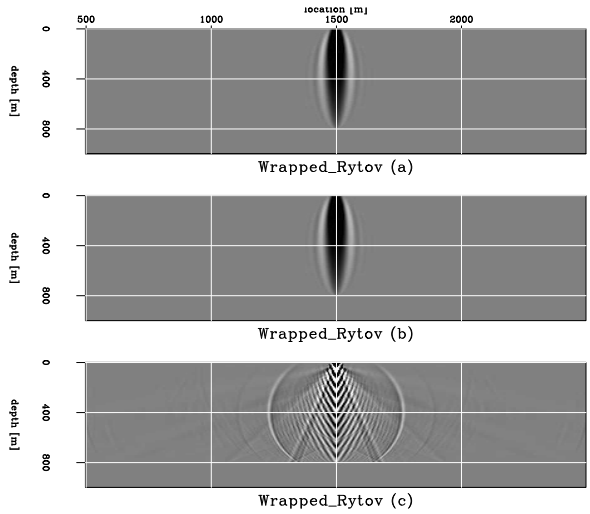

Figure 4: Fat rays for an image perturbation defined using the Rytov equation (22).The slowness anomaly is gradually increasing from (a) to (c). The phases are not unwrapped, thus the largest anomaly is not described correctly. paul1-RYTOV3b.xbsryt [CR]

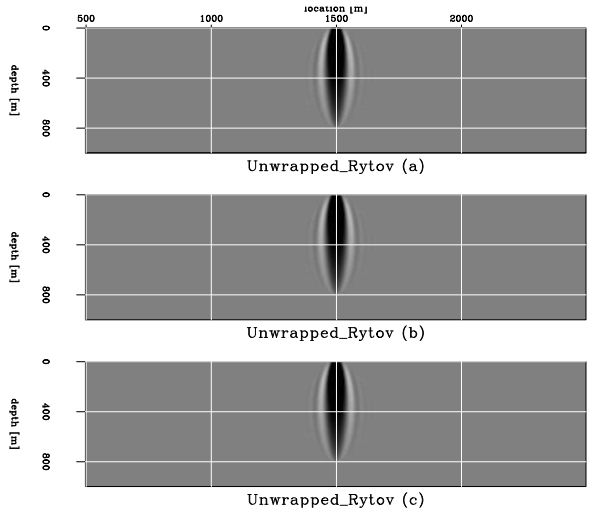

Figure 5: Fat rays for an image perturbation defined using the Rytov equation (22).The slowness anomaly is gradually increasing from (a) to (c). The phases are unwrapped, thus all anomalies are described correctly. paul1-RYTOV3b.xbsunw [CR]

perturbation decreases with increasing $\Delta\rho$.

Figure 7 is a schematic illustration of the transformation implied by equation (23). We can create enhanced images either by nonlinear residual migration, or by a first-order linearization around the background image. In principle, the accuracy of this approximation decreases with increasing $\Delta\rho$. Therefore, in practice we cannot go arbitrarily far from any given background image and we need to run several non-linear iterations involving slowness inversion, re-migration and re-linearization.

Figure 8 is a summary of fat rays computed using the methods described in the preceding section. The magnitude of the slowness anomaly increases from left to right. From bottom to top we show the fat rays for the Born definition, the Rytov definition without phase unwrapping, the Rytov definition with phase unwrapping, and the differential definition.

The four panels on the left are identical, since all methods work as well for small anomalies. In the middle four panels, the fat ray obtained with the Born definition starts to break,

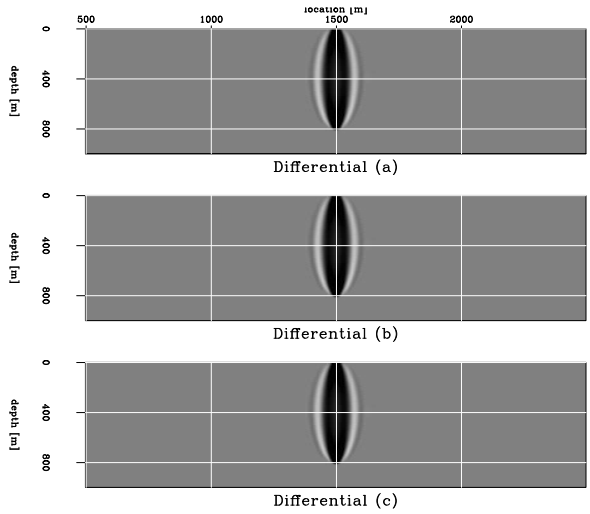

Figure 6: Fat rays for an image perturbation defined using the differential equation (23).The slowness anomaly is gradually increasing from (a) to (c). All anomalies are described correctly. paul1-RYTOV3b.xbsana [CR]

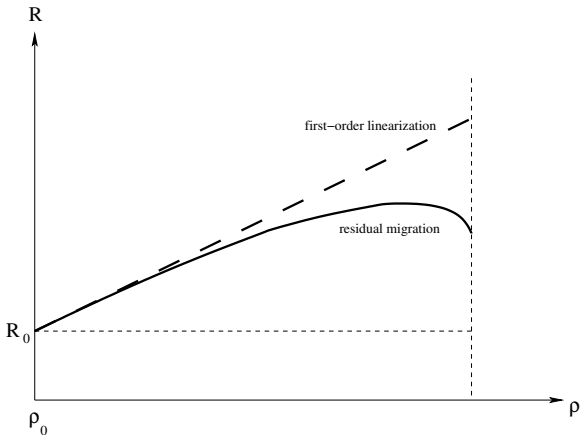

Figure 7: A sketch of the approximations done when computing image perturbations with equation (23). In this plot, each multi-dimensional image is schematically depicted by a point. We compute a linear approximation of an image corresponding to a spatially varying ρ from the gradient information computed on the background image and the $\Delta\rho$ picked from a suite of images. The accuracy of the linear approximation decreases with increasing $\Delta\rho$. paul1-dif [NR]

while the Rytov (with and without phase unwrapping) and differential approaches work well. Finally, the panels on the right correspond to the highest anomaly, when only the Rytov with phase unwrapping and differential methods work.

CONCLUSIONS

We analyze various options for computing image perturbations for wave-equation migration velocity analysis. Our three choices are Born (amplitude difference), Rytov (phase difference) and differential image perturbations derived analytically from residual migration operators.

We show that we can use the linearized WEMVA operator to invert all three types of image perturbations. We find that Rytov WEMVA is possible if we unwrap phases, but fails without.

The differential image perturbation can be used for arbitrarily large slowness anomalies, but its accuracy decreases with deviation from the background image. For simple cases, the differential image perturbation method is equivalent with a phase-unwrapped Rytov method.

REFERENCES

Al-Yahya, K. M., 1989, Velocity analysis by iterative profile migration: Geophysics, **54**, no. 6, 718–729.

Biondi, B., and Sava, P., 1999, Wave-equation migration velocity analysis: 69th Ann. Internat. Meeting, Soc. of Expl. Geophys., Expanded Abstracts, 1723–1726.

Chavent, G., and Jacewitz, C. A., 1995, Determination of background velocities by multiple migration fitting: Geophysics, **60**, no. 02, 476–490.

Clapp, R. G., 2001, Geologically constrained migration velocity analysis: Ph.D. thesis, Stanford University.

Etgen, J., 1990, Residual prestack migration and interval velocity estimation: Ph.D. thesis, Stanford University.

Liu, W., Popovici, A., Bevc, D., and Biondi, B., 2001, 3-D migration velocity analysis for common image gathers in the reflection angle domain: 71st Annual Internat. Mtg., Soc. Expl. Geophys., Expanded Abstracts, 885–888.

Mosher, C., Jin, S., and Foster, D., 2001, Migration velocity analysis using angle image gathers: 71st Annual Internat. Mtg., Soc. Expl. Geophys., Expanded Abstracts, 889–892.

Sava, P., and Biondi, B., 2003, Analytical image perturbations for wave-equation migration velocity analysis: 65th Mtg., Eur. Assoc. Geosc. Eng., Abstracts.

Sava, P., and Fomel, S., 2002, Wave-equation migration velocity analysis beyond the Born approximation: 72nd Ann. Internat. Mtg., Soc. of Expl. Geophys., Expanded Abstracts, 2285–2288.

Sava, P., and Symes, W. W., 2002, A generalization of wave-equation migration velocity analysis: SEP–**112**, 27–36.

Sava, P., 2000, Prestack Stolt residual migration for migration velocity analysis: 70th Ann. Internat. Mtg., Soc. of Expl. Geophys., Expanded Abstracts, 992–995.

Sava, P., 2003, Prestack residual migration in the frequency domain: Geophysics, **67**, no. 2, 634–640.

Stolt, R. H., 1996, Short note–a prestack residual time migration operator: Geophysics, **61**, no. 2, 605–607.

Symes, W. W., and Carazzone, J. J., 1991, Velocity inversion by differential semblance optimization: Geophysics, **56**, no. 5, 654–663.

Woodward, M. J., 1992, Wave-equation tomography: Geophysics, **57**, no. 01, 15–26.

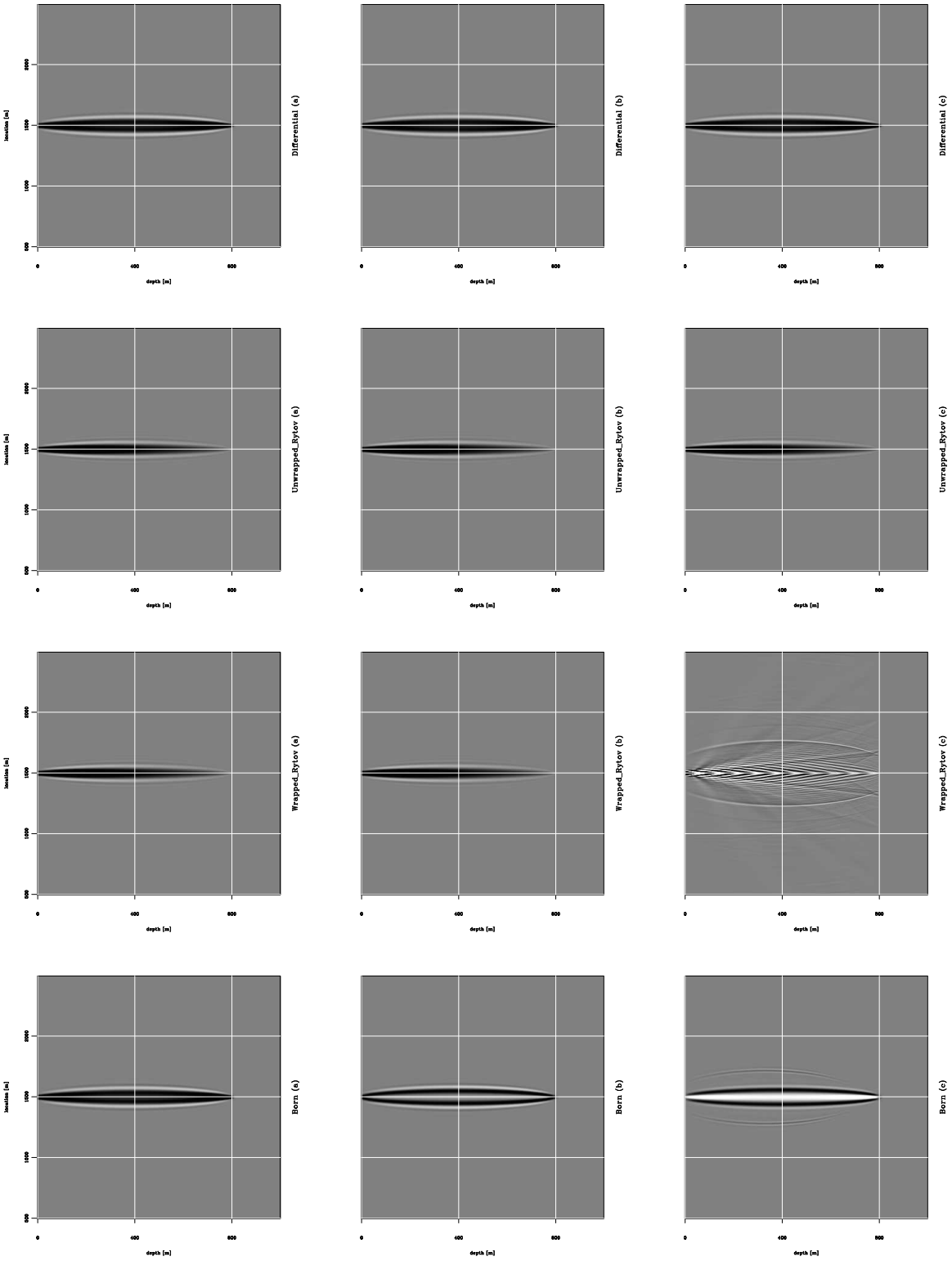

Figure 8: Summary plot for WEMVA using image perturbations constructed with different methods and with anomalies of increasing magnitude. From bottom to top we show the fat rays for the Born definition, the Rytov definition without phase unwrapping, the Rytov definition with phase unwrapping, and the differential definition. The magnitude of the slowness anomaly increases from left to right. paul1-RYTOV3b.dsall [CR]